Biochimica et Biophysica Acta xxx (2010) xxx–xxx

Contents lists available at ScienceDirect

Biochimica et Biophysica Acta

journal homepage: www.elsevier.com/locate/bbamem

Surface-induced phase separation of a sphingomyelin/cholesterol/ganglioside GM1-planar bilayer on mica surfaces and microdomain molecular conformation that accelerates Aβ oligomerization

Yanli Mao [a,b,1], Zhiguo Shang [c,1], Yosuke Imai [d], Tyuji Hoshino [d], Ryugo Tero [a,c], Motohiko Tanaka [c,e], Naoki Yamamoto [f,g], Katsuhiko Yanagisawa [g], Tsuneo Urisu [a,c,h,*]

[a] Institute for Molecular Science, Myodaiji, Okazaki 444-8585, Japan
[b] Institute of Optics and Photoelectronic Technology, Henan University, Kaifeng 475001, China
[c] Graduate University for Advanced Studies, Myodaiji, Okazaki 444-8585, Japan
[d] Department of Physical Chemistry, Chiba University, Chiba 263-8522, Japan
[e] National Institute for Fusion Science, Toki 509-5292, Japan
[f] Department of Pharmacy, College of Pharmaceutical Sciences, Ritsumeikan University, Noji, Higashi, Kusatsu, Shiga 525-8577, Japan
[g] Department of Alzheimer's Disease Research, National Institute for Longevity Sciences, National Center for Geriatrics and Gerontology, Obu 474-8522, Japan
[h] JST, CREST, Institute for Molecular Science, Myodaiji, Okazaki 444-8585, Japan

ARTICLE INFO

Article history:
Received 21 September 2009
Received in revised form 7 February 2010
Accepted 1 March 2010
Available online xxxx

Keywords:
Lipid bilayer
Sphingomyelin
Cholesterol
Ganglioside GM1
Molecular dynamics
Phase separation

ABSTRACT

Ganglioside GM1 mediates the amyloid beta (Aβ) aggregation that is the hallmark of Alzheimer's disease (AD). To investigate how ganglioside-containing lipid bilayers interact with Aβ, we examined the interaction between Aβ40 and supported planar lipid bilayers (SPBs) on mica and SiO_2 substrates by using atomic force microscopy, fluorescence microscopy, and molecular dynamics computer simulations. These SPBs contained several compositions of sphingomyelin, cholesterol, and GM1 and were treated at physiological salt concentrations. Surprisingly high-speed Aβ aggregation of fibril formations occurred at all GM1 concentrations examined on the mica surface, but on the SiO_2 surface, only globular agglomerates formed and they formed slowly. At a GM1 concentration of 20 mol%, unique triangular regions formed on the mica surface and the rapidly formed Aβ aggregations were observed only outside these regions. We have found that some unique surface-induced phase separations are induced by the GM1 clustering effects and the strong interactions between the GM1 head group and the water layer adsorbed in the ditrigonal cavities on the mica surface. The speed of Aβ40 aggregation and the shape of the agglomerates depend on the molecular conformation of GM1, which varies depending on the substrate materials. We identified the conformation that significantly accelerates Aβ40 aggregation, and we think that the detailed knowledge about the GM1 molecular conformation obtained in this work will be useful to those investigating Aβ–GM1 interactions.

1. Introduction

The ganglioside GM1 (GM1) has a ceramide backbone and a large complex head group containing a pentasaccharide. Gangliosides contribute to numerous cellular functions in the nervous system, such as signal transduction, neuronal differentiation, and the formation of axons, dendrites, and synapses [1,2]. In addition, GM1 forms a seed complex with amyloid beta (Aβ) and accelerates the formation of toxic Aβ oligomers and fibrils implicated as a cause of neuronal death in Alzheimer's disease (AD) [3–11]. In the presence of GM1, Aβ undergoes a conformational change from random coil to α-helix and/or β-sheet, resulting in the aggregation of Aβ [7]. The trisialoganglioside GT1b also facilitates fibrillization of Aβ, although not as effectively as GM1 [7]. The Aβ binding of several photopolymerized oligosaccharides containing sialic acid was investigated in an effort to develop new ways to prevent Aβ toxicity [12]. Sugar moieties, especially sialic acid moieties, were found to contribute to the aggregation of Aβ, and the interaction between Aβ and gangliosides/sialic acids seems to be complex. Aβ–ganglioside interaction depends on pH and NaCl concentration. At pH 7, gangliosides induce α-helical structure in Aβ and thereby diminish fibrillogenesis [13]. Even though the complexity of the Aβ–ganglioside interaction implies that it cannot be understood without analyzing the structures of the interacting molecules, the detailed molecular conformations of neither GM1 nor sugar moieties have been investigated in relation to this interaction.

Sugar specificity has also been reported for the coil-to-β structural transition of the prion peptide [14]. O-linked α-GalNAc at Ser-135 inhibits fibril formation of prion peptides at physiological salt concentrations, whereas the peptide with the same sugar at Ser-132

* Corresponding author. Fax: +81 564 55 7327.
E-mail address: urisu@ims.ac.jp (T. Urisu).
[1] These authors contributed equally to this work.

0005-2736/$ – see front matter © 2010 Elsevier B.V. All rights reserved.
doi:10.1016/j.bbamem.2010.03.003

promoted fibril formation. Although little information regarding molecular interactions between sugars and Aβ or prion protein (PrPc) is available, recent studies using molecular dynamics (MD) simulations [15–17], NMR[18,19], and atomic force microscopy (AFM) [20,21] are relevant because they describe the oligomer structure and dynamics during Aβ and fibril elongation. Thus, the combination of MD simulations and AFM or NMR observations is extremely useful for understanding the conformations and interactions of complex biomolecules.

In recent years, the existence and roles of membrane microdomains, such as rafts in the plasma membrane, have drawn much attention [22]. These microdomains are enriched in glycosphingolipids, sphingomyelin (SM), and cholesterol (CHOL) and have been proposed to play important roles in signal transduction, cellular transport, and lipid sorting [23,24]. Common eukaryotic membranes contain about 50% (mole fraction) sphingolipids and phospholipids and up to 40% CHOL [25]. It is reported that GM1 molecules are concentrated in caveolae by several percentage or higher concentrations [26].

Supported planar lipid bilayers (SPBs) [27–32] are *in vitro* model systems for investigating how cell membranes influence protein–lipid and cell–cell interactions. The advantage of the SPB system is that it is compatible with advanced techniques for surface characterization, including AFM [31], fluorescence microscopy (FM) [28–31], infrared spectroscopy [30], and secondary ion mass spectrometry [32]. AFM is an especially powerful technique for obtaining information about the molecular or microdomain conformations of SPBs [31–34].

In this work, we have investigated the interaction between Aβ40 and GM1 in SPBs with several SM/CHOL/GM1 compositions, some of which had GM1 concentrations close to physiological, by using *in situ* AFM, FM, and MD simulations. These SPBs were formed by vesicle fusion on SiO_2 and mica surfaces. The aggregation speeds and morphologies of the Aβ40 agglomerates differed significantly between SiO_2 and mica surfaces. The surprisingly high-speed aggregation observed for all GM1 concentrations examined on the mica surface is attributed to the molecular conformation of GM1 cluster domains induced by the clustering effects of GM1 molecules and the strong interactions between the GM1 head group and the water molecules bound closely to the ditrigonal cavities in the mica surface. The detailed molecular conformation of GM1 in each of the domains in SPBs on SiO_2 and mica surfaces has been determined, and these results represent an important step in the precise molecular characterization of Aβ–GM1 interactions.

2. Materials and methods

2.1. Materials

SM (porcine brain, Avanti), CHOL (Sigma), GM1 (bovine brain, Sigma), NBD-C6-SM (NBD-SM) (Molecular Probes), thioflavin T (Sigma), Alexa Fluor 555 cholera toxin subunit B (CTX-B) (Molecular Probes), and Aβ40 protein (Peptide Institute) were used as delivered.

2.2. SPB preparation

The SPBs were prepared as follows: all lipids were dissolved in chloroform/methanol (1:1, v/v) and subsequently mixed at predetermined ratios. The concentration of the NBD-SM was 1% (mol/mol). The lipid mixtures were dried in a rotary evaporator and then stored overnight under high vacuum. After the solvents were evaporated, the lipid film was rehydrated to a final concentration of 0.12 mg/ml by using a buffer solution (150 mM NaCl, 10 mM HEPES, 2 mM $CaCl_2$, pH 7.4), freeze–thawed, and sonicated at 60 °C to obtain small unilamellar vesicles (SUVs). Five hundred microliters of the SUV suspension thus obtained was poured on freshly cleaved mica substrates 20 mm in diameter. The liposomes were allowed to fuse at room temperature for 30 min and then heated to 70 °C for 15 min. After the sample cooled to room temperature, it was rinsed with the buffer solution.

2.3. SiO_2 substrate preparation

SiO_2 was formed by wet oxidation of a mirror-polished Si(100) wafer. The Si(100) wafers were cleaned by successive treatment with the following solutions: concentrated $H_2SO_4 + H_2O_2$(30%) (4:1 by volume), $NH_4OH + H_2O_2$(30%) + H_2O (1:1:3), HF(5%), and concentrated $HCl + H_2O_2$(30%) + H_2O (1:1:4). The cleaned surface was covered with a chemically oxidized SiO_2 layer with surface roughness $Ra = 0.14 \pm 0.02$ nm.

2.4. Preparation of Aβ40 solution

The Aβ40 protein was dissolved in a 0.02% ammonia solution. The solution was then centrifuged at 100,000 rpm for 3 h (Beckman Instruments) to remove undissolved peptide aggregates that might act as nucleation sites. The supernatant (final concentration = 500 μM) was collected and stored in aliquots at −20 °C until use.

2.5. AFM and fluorescence microscopy

AFM was performed in the buffer solution using a SPI3800 scanning probe microscopy system (Seiko Instruments Inc.) in the tapping mode using a Si_3N_4 cantilever. The spring constant and the resonance frequency of the cantilevers were 1.6 N/m and 26 kHz, and all bilayers were imaged at room temperature. A fluorescence microscope (Olympus) equipped with a digital CCD camera (Nikon DS-2MBW) was used for collecting fluorescence images. Once the formation of the SPB was confirmed by AFM and FM, in some experiments, a small volume of concentrated Alexa 555 CTX-B stock solution (1.0 mg/ml) was injected into the chamber and permitted to distribute evenly by diffusion. The final concentration of CTX-B was estimated to be 2.0 μg/ml.

2.6. MD simulation method

The chemical structures of lipid molecules were constructed with the program GaussView. The program Visual Molecular Dynamics (VMD) [35] and an in-house program called GLYMM were used to assemble dozens of lipid molecules to form several model membranes: model (a) consisting of 32 SM molecules, 32 CHOL molecules, and 16 GM1 molecules (SM/CHOL/GM1 (40:40:20)); model (b) consisting of 32 SM molecules and 32 CHOL molecules (SM/CHOL (50:50)); model (c) consisting of 32 GM1 molecules and 32 CHOL molecules (GM1/CHOL (50:50)); and four models (d) for extremely low GM1 densities: 2 GM1 + 30 SM + 32 CHOL, 4 GM1 + 28 SM + 32 CHOL, 6 GM1 + 26 SM + 32 CHOL, and 8 GM1 + 24 SM + 32 CHOL. The CHARMM27 force field for lipids and the CHARMm force field for small organic molecules were used, and all simulations were performed using the NAMD (version 2.5) program. In each calculation, water boxes 4–5 nm thick were added to both upper and lower sides of the starting bilayer model. In the MD simulations, unfavorable contacts between molecules were first removed by energy minimization. Then the system was heated to 37 °C, and runs were executed to equilibrate the system at a constant temperature of 37 °C and a constant pressure of 1 atm. The bilayer thickness was defined as the average distance between N atoms in the upper and lower leaflets of SPBs. In SPBs containing GM1, the N atoms used to define thickness were those in N-acetylneuraminic acid (Neu5Acα).

Please cite this article as: Y. Mao, et al., Surface-induced phase separation of a sphingomyelin/cholesterol/ganglioside GM1-planar bilayer on mica surfaces and microdomain..., Biochim. Biophys. Acta (2010), doi:10.1016/j.bbamem.2010.03.003

3. Results

3.1. Surface morphologies of SM/CHOL/GM1-SPBs on freshly cleaved mica and SiO_2 substrates

Flat SPBs with a 40:40:20 SM/CHOL/GM1 composition were easily obtained on both SiO_2 [36] and mica substrates. On mica surfaces, vesicles fused to form a flat and uniform membrane immediately after preparation at 70 °C (Fig. 1a). Following incubation at 37 °C for 24 h, triangular regions often appeared (Fig. 1b). The triangular regions A and A′ in Fig. 1b were, respectively, 2.6 ± 0.2 and 1.5 ± 0.2 nm higher than the surrounding area B. After longer (36 h) incubation at 37 °C, the phase separation inside the triangular region became more evident, and the regions C and C′ in Fig. 1c were, respectively, 2.4 ± 0.3 and 0.64 ± 0.15 nm higher than area B. The heights and areas of the triangular regions thus differed from sample to sample (Fig. S1, Supplementary material). The triangular regions could be classified into two kinds according to height: SM-rich regions 2.4 ± 0.8 nm high containing a small number of GM1 molecules and SM-rich regions 1.3 ± 0.8 nm high containing no GM1. We think the triangular regions are formed by coalescence of SM-rich and GM1-rich microdomains formed by the phase separations on the mica surface as discussed in Section 4.1, and we think that the significant variation of the shapes of the triangular regions is a result of the coalescence being induced by the slow and long-distance movement of the microdomains and thus easily influenced by uncontrollable slight changes of room temperature and surface conditions.

We also examined SPBs with other compositions: although 55:40:5 SM/CHOL/GM1, 50:40:10 SM/CHOL/GM1, and 50:50 CHOL/GM1 formed flat SPBs by vesicle fusion (Fig. S2a for GM1 = 5 mol%, Supplementary material), unfused vesicles or secondary bilayers or defects were sometimes observed (data not shown). Triangular regions such as those observed in the 20 mol% GM1 SPBs were not formed in the SPBs with these compositions. On SiO_2 surfaces, on the other hand, 45:40:15, 40:40:20, and 35:40:25 SM/CHOL/GM1 compositions all form flat and homogeneous SPBs regardless of the length of the incubation time [36]. Flat secondary bilayers 6.20 ± 0.2 nm thick often formed from compositions of 40:40:20 (Fig. 1d) and 45:40:15 (Fig. 2d in ref. [36]). At compositions of 55:40:5 and 50:40:10, SPBs were obtained but their morphologies were defective [36]. SPBs from a composition of CHOL/GM1 (50:50) displayed defects ≈ 1 nm deep, and it was not clear whether the lipid films were or were not bilayers (Fig. S2b, Supplementary material).

3.2. Assay using fluorescence-dye-labeled SM and CTX-B

We carried out the assay using fluorescence-dye-labeled SM (NBD-SM) and CTX-B (Alexa 555 CTX-B) mainly for the 20 mol% GM1 case, in which clearly triangular regions were observed on the mica surface (Fig. 2a–d). The triangular regions in fluorescence images of SPBs formed from 40:40:20 SM/CHOL/GM1 containing 1% (mol/mol) NBD-SM are brighter than the surrounding area (Fig. 2a), which is consistent with the enrichment of SM in the triangular regions. The NBD-SM in the center of the image was photobleached, and fluorescence recovery (FRAP) was monitored in order to test the fluidity of the SPB (Fig. 2e). Almost complete recovery was observed after 12 min, but careful observation revealed that the shape of the dark region (that is, the area outside the triangular region) was constant during the FRAP observation even though the diffusion of NBD-SM was evident. This indicates that the whole lipid bilayer system is in the liquid phase, since the observed recovery time is much faster than that expected for the gel phase, in which the diffusion coefficient is several orders of magnitude smaller than that in the liquid phase [37]. The triangular region including the inside microstructures continuously changed with increasing incubation time as shown in Fig. 1a, b, and c. This also indicates that the triangular regions are formed by liquid–liquid phase separation. Both the triangular region and the surrounding region are in the liquid phase because of the high concentration of CHOL [38].

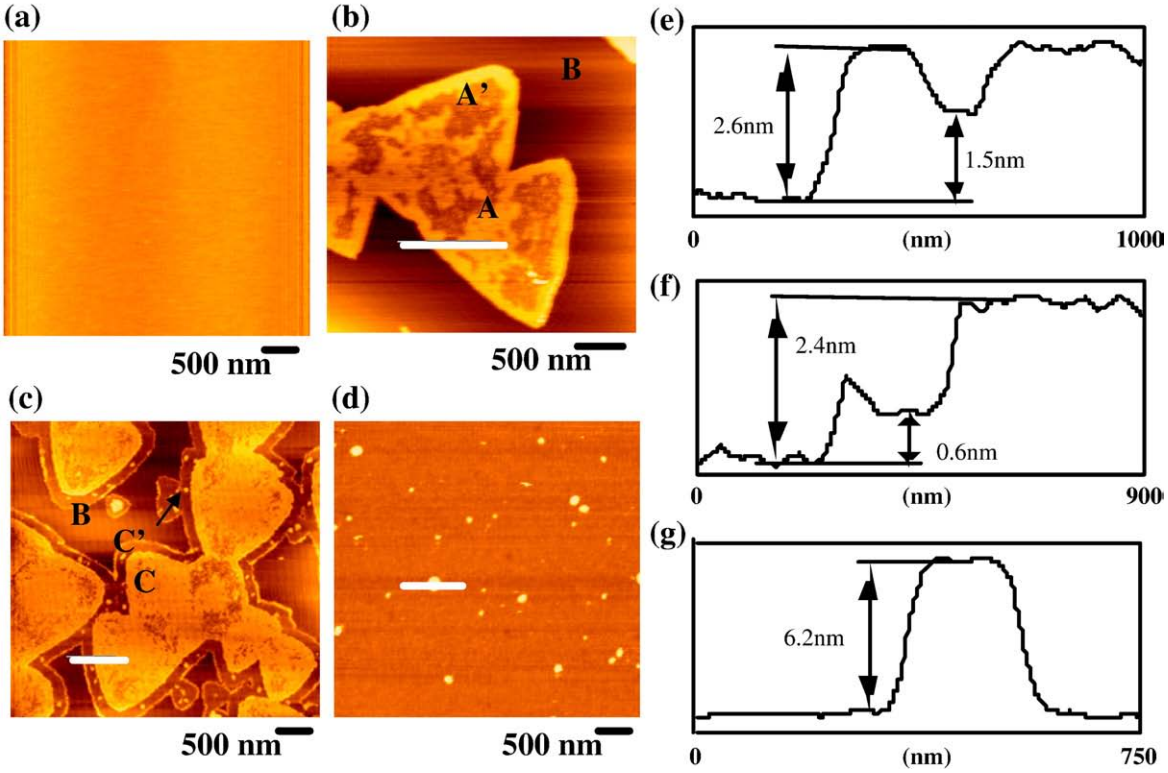

Fig. 1. AFM images of SM/CHOL/GM1 (40:40:20)-SPBs on mica and SiO_2. (a) SPB on freshly cleaved mica that was incubated in a vesicle suspension at RT for 30 min and at 70 °C for 15 min. (b) The SPB in (a) following incubation at 37 °C for 24 h. (c) The SPB in (a) following incubation at 37 °C for 36 h. (d) An SPB on SiO_2 obtained under the same conditions as the SPB shown in panel (b). Panels (e), (f), and (g) are, respectively, line profiles of the SPBs shown in panels (b), (c), and (d).

Please cite this article as: Y. Mao, et al., Surface-induced phase separation of a sphingomyelin/cholesterol/ganglioside GM1-planar bilayer on mica surfaces and microdomain..., Biochim. Biophys. Acta (2010), doi:10.1016/j.bbamem.2010.03.003

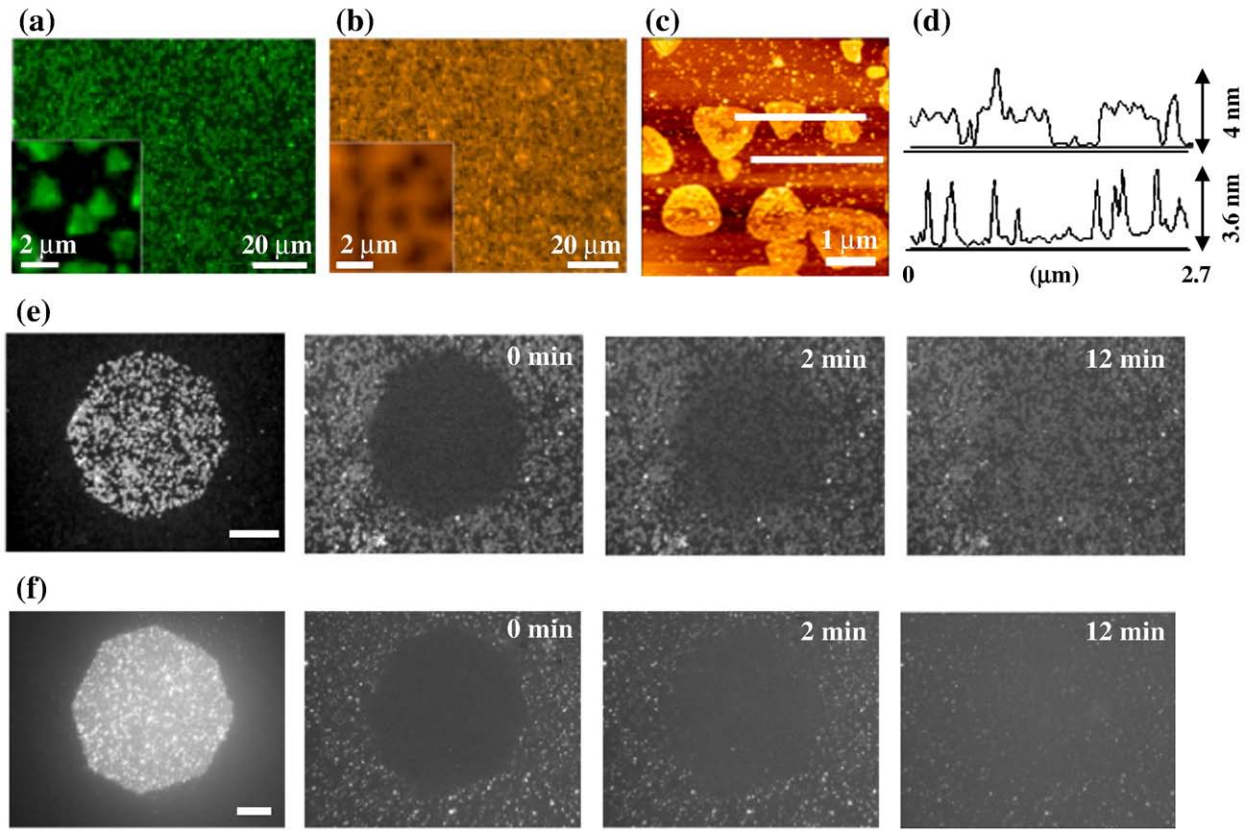

Fig. 2. SM/CHOL/GM1 (40:40:20)-SPB images obtained by (a) FM, (b) FM, and (c) AFM. (a) SPB containing 1% (mol/mol) NBD-SM after the formation of triangular regions on mica. (b, c) Triangular regions on mica following the addition of Alexa 555 CTX-B. (d) The line profiles for the white lines in panel (c). The areal density of protrusions 2.9 ± 0.6 nm high assigned to the aggregation of CTX-B and GM1 is $\approx 20.0/\mu m^2$ outside the triangular regions in panel (c) and $\approx 2.5/\mu m^2$ inside the triangular regions in panel (c). (e) Sequential FM images (obtained using a 60× objective lens) of the SPB on the mica substrate after photobleaching (scale bar = 60 μm). (f) Sequential FM images (obtained using a 40× objective lens) of for the SPBs, without secondary bilayers, on the SiO_2 substrate after photobleaching (scale bar = 40 μm). The fluorescence from the bleached area recovered following lateral diffusion of NBD-SM.

The distribution of GM1 was visualized with CTX-B, which strongly associates with GM1 [30,31,39]. When the SM/CHOL/GM1(40:40:20) SPBs with triangular regions were incubated in a buffer solution containing CTX-B (2.0 μg/ml) for 30 min at room temperature (RT), the bright fluorescence of Alexa 555 CTX-B covered the surface punctuated by many dark regions (Fig. 2b) that corresponded to triangular regions. Correspondingly, small protrusions were observed in the AFM images (Fig. 2c and d). The areal densities of these protrusions inside and outside the triangular regions in Fig. 2c, were, respectively $2.5/\mu m^2$ and $20.0/\mu m^2$. The interaction between CTX-B and GM1 mixed in the POPC bilayer was investigated for GM1 concentrations of 0.02–10% and CTX-B concentrations of 0–6 nM by Shi et al. [31], who reported that the apparent equilibrium dissociation constant Kd of the GM1-CTX-B aggregation reaction increased monotonically from 0.23 to 0.86 nM as the GM1 concentration increased from 0.1 to 10.0 mol%. This indicates that although the number density of GM1-CTX-B agglomerates increases with increasing GM1 concentration, the clustering effect causes the aggregation efficiency to decrease with increasing GM1 concentration. If this relation could be applied qualitatively to the system we investigated, the areal densities of agglomerates (protrusions) observed inside and outside the triangular regions, respectively, $2.5/\mu m^2$ and $20.0/\mu m^2$, would indicate that the GM1 concentration in a triangular region was much less than 1/10 of that outside the region.

The average height of these protrusions, 2.9 ± 0.6 nm was greater than that of the triangular regions whose line profiles are shown in Fig. 2d (2.2 ± 0.2 nm). These small protrusions result from the aggregation of CTX-B and GM1 [39]. We conclude from the fluorescence and CTX-B assay data (Fig. 2b, c, and d) that GM1 molecules are distributed mainly outside of the triangular regions. In similar experiments with NBD-SM and CTX-B on SPBs on SiO_2 substrates, SM and GM1 were distributed uniformly and the SPBs were in the liquid phase (Fig. 2f).

3.3. Interaction between Aβ40 and SM/CHOL/GM1-SPBs

SPB morphologies were observed after a 20 μM Aβ40 solution had been added to SM/CHOL/GM1(40:40:20) SPBs on mica and SiO_2 substrates immediately after their formation and the samples had been incubated at 37 °C for 36 h. Significant aggregation of Aβ40 and disruption of the bilayer were clearly observed (Fig. 3a and b). On SPBs lacking GM1, in contrast, there was no trace of Aβ aggregation under the same conditions (data not shown). After a 20 μM Aβ40 solution had been added to SM/CHOL/GM1(40:40:20) SPBs and SM/CHOL(50:50) SPBs on mica surfaces immediately after their preparation and the samples were incubated at 37 °C for 36 h, Aβ aggregation was investigated by thioflavin T assay as shown in Fig. 3c and d. Brighter particles indicating the presence of amyloid fibrils were observed only in the SM/CHOL/GM1(40:40:20) SPBs (Fig. 3c). No fluorescence signals were observed in the SM/CHOL (50:50) SPBs without GM1 (Fig. 3d). Similar results were obtained on the SiO_2 surface (data not shown). These results show that GM1 was required for the observed Aβ aggregation. To investigate this aggregation in greater detail, we prepared samples with more dilute Aβ. When we added a 2 μM Aβ solution to SPBs on the mica surface after the triangular regions appeared, Aβ aggregation was most evident outside the triangular regions (Fig. 4a and b). The edges of the triangular regions were also sites where Aβ aggregation began.

Please cite this article as: Y. Mao, et al., Surface-induced phase separation of a sphingomyelin/cholesterol/ganglioside GM1-planar bilayer on mica surfaces and microdomain..., Biochim. Biophys. Acta (2010), doi:10.1016/j.bbamem.2010.03.003

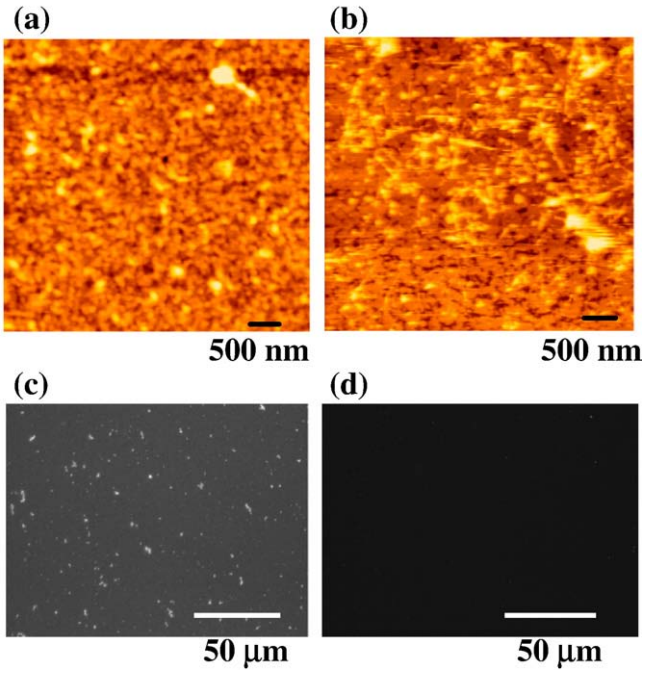

Fig. 3. AFM images of Aβ40 protein aggregation on SM/CHOL/GM1 (40:40:20)-SPBs incubated at 37 °C for 36 h on (a) mica and (b) SiO_2 surfaces. (c) FM image of the SPB shown in panel (a) after addition of thioflavin T solution (5 μM). (d) FM images after addition of thioflavin T solution (5 μM) to SM/CHOL (50:50) SPBs on a mica surface for which Aβ40 (20 μM) is added under the same conditions as panels (a) and (b). Agglomerates of Aβ are observed in panel (c) but not in panel (d).

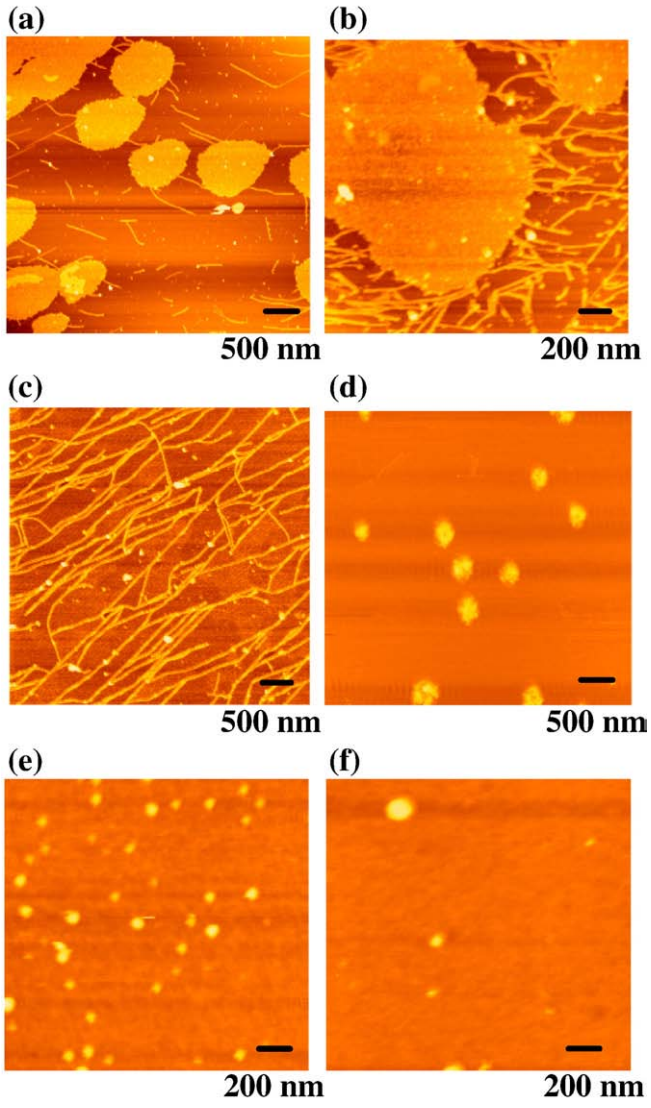

Fig. 4. (a, b) The time course of Aβ aggregation on the SM/CHOL/GM1 (40:40:20)-SPBs on mica measured by AFM. Aβ solution (2 μM) was added after the formation of trianglular regions. (a) One-hour incubation at 37 °C. (b) Twelve-hour incubation at 37 °C. (c) Aβ aggregation on the GM1/CHOL (50:50)-SPB on a mica substrate after the 12-h incubation at 37 °C. Aβ solution was added immediately after the formation of the SPB. (d) The AFM image obtained just after the formation of a GM1/CHOL (50:50)-SPB on mica. (e, f) AFM images of Aβ40 aggregation on SM/CHOL/GM1 (40:40:20)-SPBs on SiO_2. Aβ solution (2 μM (e) and 1 μM (f)) was added to the SPBs immediately after its formation. Protrusions observed in panels (e) and (f) are globular agglomerates of Aβ40 that are 3.5 ± 1.2 nm high.

Clear Aβ aggregation was not observed on the surface of the triangular regions.

The fluorescence images in Fig. 2a and b demonstrate that outside of the triangular regions GM1 is dominant and the SM concentration is low. To examine the dependency of Aβ aggregation on GM1 outside of triangular regions, where most of the GM1 is, we also added a 2 μM Aβ solution to GM1/CHOL(50:50) SPBs on mica surfaces immediately after the SPB formation. Aggregating fibrils were present on this surface (Fig. 4c). Interestingly, with this composition, some phase separations were also observed on the mica surface (Fig. 4d). Similar results were also obtained when a 2 μM Aβ solution was added to SM/CHOL/GM1 (55:40:5) SPBs on mica surfaces (Fig. S2d, Supplementary materials). These fibrils observed on the mica surfaces tended to grow in only one direction.

In contrast to what was seen on the mica surfaces, only small protrusions and no fibrils were seen on SiO_2 substrates after 2 and 1 μM solutions of Aβ40 were added and the samples were incubated at 37 °C for 36 h (Fig. 4e and f). The small protrusions on the SiO_2 substrates were mainly globular aggregates of Aβ40 with an average height of 3.5 ± 1.2 nm. These protrusions can be clearly distinguished from those formed by phase separation (Fig. 4d), which have triangular or rounded triangular shapes similar to those of the regions shown in Fig. S1. These agglomerates (shown in Fig. 4e and f) are also easily distinguished from the second bilayer seen in Fig. 1d by their heights (Supplementary information Fig. S3) and were easily removed by the AFM tip. Fibril formation was not observed for any of the compositions examined on SiO_2 surfaces.

3.4. Concentration dependence of the Aβ aggregation reaction

The dependence of the Aβ agglomerate formation on the Aβ concentration is shown in Fig. 5a–c for mica surface and in Fig. 5d–f for SiO_2 surfaces. In these cases, the Aβ solution was added just after the formation of the lipid bilayers (not after the appearance of triangular regions). The Aβ concentrations for a and d, b and e, and c and f were, respectively, 20, 2, and 1 μM. The concentration dependences with Aβ addition after the formation of triangular regions were examined only for 20 and 2 μM solutions (Fig. 5g and h).

We did not evaluate these Aβ concentration dependences quantitatively, but these results clearly show that on both mica and SiO_2 surfaces, the rates at which Aβ agglomerates forms depend on the Aβ concentration nonlinearly. It is considered that the lipid bilayer structure is destroyed by the high density of Aβ agglomerates in the case of 20 μM. We think that this nonlinear dependence of the reaction rate is explained by a reaction model in which soluble oligomers (Aβn) are formed and react with the cell membrane surface to form fibrillar aggregates (on the mica surface) or globular aggregates (on the SiO_2 surface). Interestingly, this reaction model of soluble oligomers (Aβn) formation is consistent with the report that

Please cite this article as: Y. Mao, et al., Surface-induced phase separation of a sphingomyelin/cholesterol/ganglioside GM1-planar bilayer on mica surfaces and microdomain..., Biochim. Biophys. Acta (2010), doi:10.1016/j.bbamem.2010.03.003

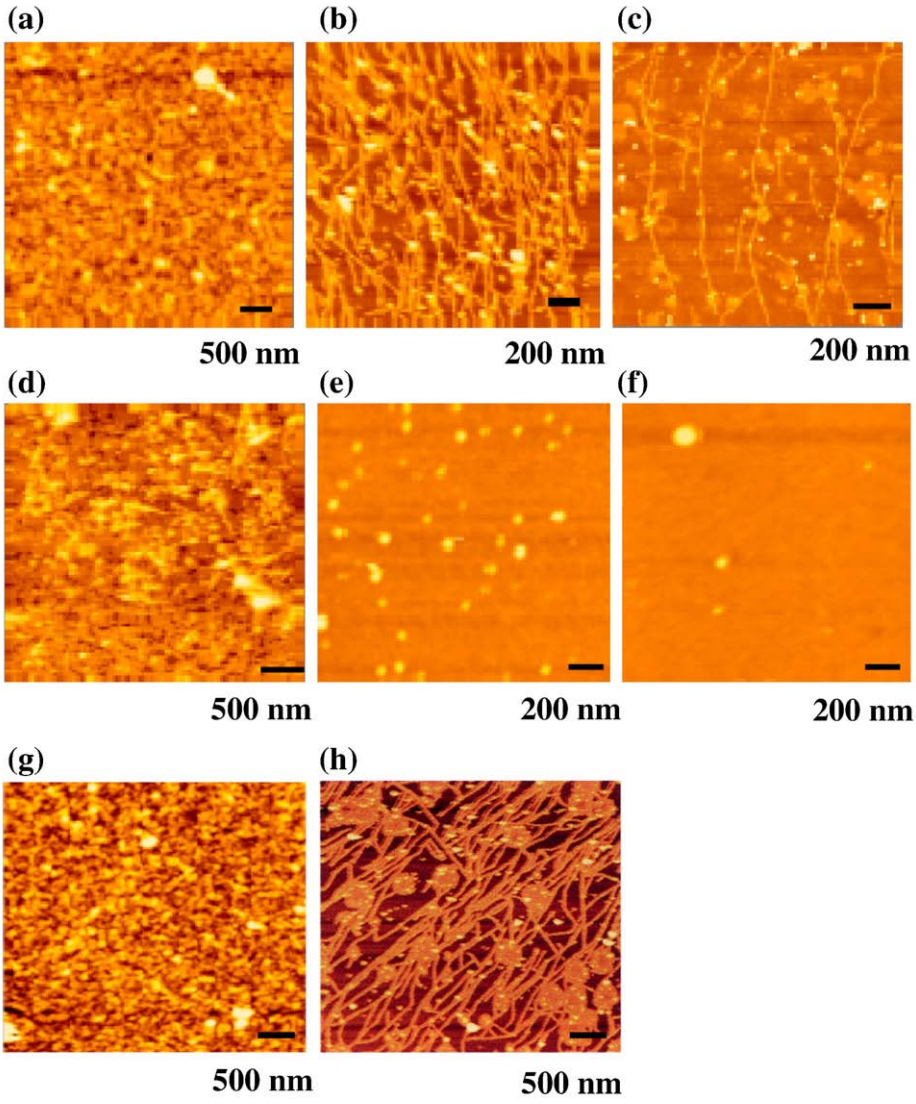

Fig. 5. AFM images showing the concentration dependence of Aβ agglomerate formation. Panels (a), (b), and (c) are, respectively, for Aβ concentrations of 20, 2, and 1 μM on mica surfaces. Panels (d), (e), and (f) are, respectively, for Aβ concentrations of 20, 2, and 1 μM on SiO_2 surfaces. In these cases, the Aβ solutions were added just after the lipid bilayer formations (not after the triangular region formations). Panels (g) and (h) are, respectively, for 20 and 2 μM Aβ solutions added just after the formation of triangular regions in SPBs on mica surfaces.

the Aβ oligomers extracted from Alzheimer's disease brains are the synaptotoxic species [40].

4. Discussion

4.1. Relation between domain structure and Aβ aggregation.

The SM/CHOL/GM1(40:40:20) SPBs on the SiO_2 surface were 6.20 ± 0.2 nm thick (Fig. 1g). Since the conformation of a GM1 molecule is easily altered by the internal rotation around a chemical bond formed by carbon sp3 orbitals, the SPB thickness is thought to depend on the molecular conformation of GM1—that is, on the arrangement of the large and long GM1 head group relative to the ceramide part—and 6.20 nm is almost the greatest thickness of a SPB containing GM1 (see Fig. 6). The area outside the triangular region is GM1-rich, and the area inside the triangular region is further separated into phases containing small number of GM1 and lacking GM1. The large difference between the heights of the two GM1-containing regions B and C in Fig. 1c (2.4 nm) indicates that, in the GM1-containing region C in Fig. 1c of the triangular region, the SPB also has the greatest thickness ($\approx$6.2 nm). Otherwise, it is impossible to explain the thickness of the GM1-rich region outside the triangular region. This means that the GM1 molecular conformation in areas outside the triangular regions is largely different from that in the SPB on the SiO_2 surface or the region C on the mica surface.

While the results of several experiments have shown that GM1 promotes the aggregation of Aβ [3–11], how this aggregation might depend on the GM1 conformation is completely unknown. From the present finding that high-speed Aβ aggregation with fibril formation occurs only on the very thin bilayer region (outside the triangular region in Fig. 1c), we infer that GM1-assisted Aβ aggregation indeed depends on the conformation of GM1.

4.2. Domain structures of SPBs on SiO_2 and mica surfaces

The triangular regions in SPBs on mica surfaces are SM-rich and the surrounding areas are GM1-rich. We tried to measure the thickness of SPBs on mica and SiO_2 surfaces by digging a hole with the tip of the AFM cantilever. Although the fluidity of the SPBs made it hard to determine the exact thickness, we concluded that all the membranes shown in Fig. 1 were single bilayers (Fig. S4, Supplementary material), save for instances where second bilayers are obvious

Please cite this article as: Y. Mao, et al., Surface-induced phase separation of a sphingomyelin/cholesterol/ganglioside GM1-planar bilayer on mica surfaces and microdomain..., Biochim. Biophys. Acta (2010), doi:10.1016/j.bbamem.2010.03.003

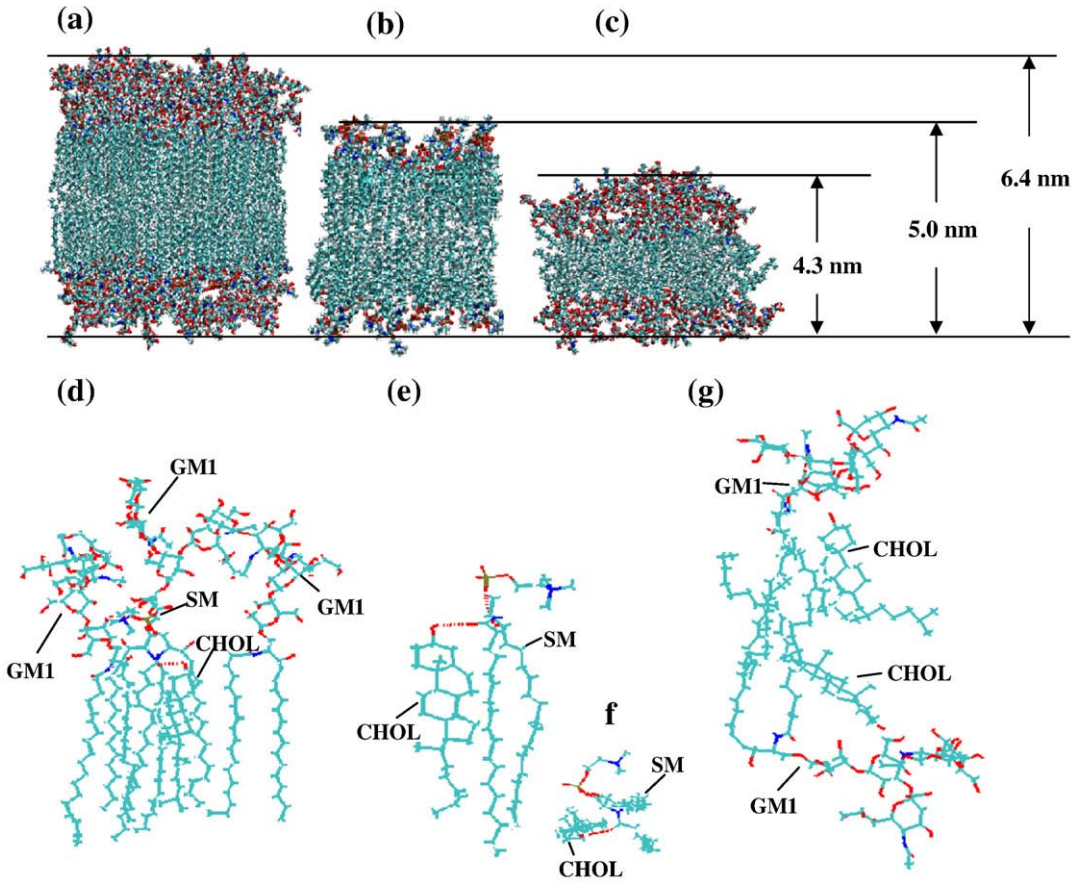

Fig. 6. Equilibrium-state SPBs obtained by MD computer simulation for (a) SM/CHOL/GM1 (40:40:20) and (b) SM/CHOL (50:50) when using the liquid-ordered phase as the starting model, and (c) the interdigitated liquid-disordered phase of CHOL/GM1 (50:50) calculated assuming hydrogen-bonding interactions with water molecules trapped in the ditrigonal cavities on the mica surface (Fig. 7). Here, the SPB was placed above the trapped water layer so that the distance between the lowest H atoms of the SPB and the upper side H-atom layer of the trapped water became 0.25 nm. The positions of O atoms were fixed. (d) Magnified image of panel (a), in which one GM1 molecule, two SM molecules, and two CHOL molecules interacting through hydrogen bonding and hydrophobic interactions are shown. (e) Magnified image of panel (b) showing the interaction of one SM molecule and one CHOL molecule. (f) Top view of panel (e). (g) Magnified image of panel (c) showing two GM1 molecules interacting with two CHOL molecules, thereby forming the interdigitated liquid-disordered bilayer. In panels (d) to (g), the colors red, blue, brown, and green, respectively, show O, N, P, and C atoms.

(Fig. 1d). To determine the molecular conformations of lipids in each domain, we used the software NAMD and performed MD simulations for (a) 40:40:20 SM/CHOL/GM1, (b) 50:50 SM/CHOL, and (c) 50:50 GM1/CHOL. In each simulation, we set a model structure and calculated 10-ns trajectories. In cases (a) and (b), the equilibrium structures were obtained using the simple liquid-ordered phase as the starting model of the bilayer (Fig. 6a and b). As a clear phase separation did not occur on the amorphous SiO_2 surface, we considered the structure of the SPB on SiO_2 surfaces to be given by the case (a) calculation. The calculated SPB thickness of 6.4 nm (Fig. 6a) is in good agreement with the observed thickness of 6.2 ± 0.2 nm (Fig. 1g). The detailed molecular structure of GM1 obtained by the calculation for case (a) is shown in Fig. 6d. GM1 molecules have the longest conformation with a "standing" head group supported by hydrogen bonding and hydrophobic interactions with surrounding SM and GM1 molecules. The triangular regions on mica surfaces shown in Fig. 1b further separate to the higher and the lower regions following longer incubations (respectively, C and C′ in Fig. 1c), where average difference between the heights of the regions C and C′ was 1.8 ± 0.2 nm (Fig. 1f). This value is close to the ≈ 1.4 nm calculated for the difference between the thicknesses of 40:40:20 SM/CHOL/GM1 (Fig. 6a) and 50:50 SM/CHOL (Fig. 6b). Because the triangular regions in Fig. 1b are SM-rich but contain some GM1 molecules (Fig. 2c and d), the change from Fig. 1b to c is likely to be a consequence of the intra-triangular-region phase separation into regions containing and lacking GM1. Therefore, the GM1 molecules in the triangular regions A in Fig. 1b and C in Fig. 1c also have the "longest" conformation (Fig. 6d). The molecular conformation of SM in region C′ in Fig. 1c is shown in Fig. 6e.

The molecular conformation of GM1 outside the triangular regions (e.g., areas B in Fig. 1b and c) is interesting. The SPB thickness in B is ≈ 4 nm, a value calculated as the difference between the thickness of region A or C in Fig. 1 (6.4 nm in Fig. 6a) determined by the longest conformation of GM1 and the difference between the heights of region C and area B (2.4 nm, Fig. 1f). This value is surprisingly small for the thickness of an SPB containing GM1. Although the exact composition of this region is hard to estimate, the region is GM1-rich, and GM1/CHOL (50:50) should therefore be a good approximation if the CHOL is distributed uniformly. The 50:50 GM1/CHOL SPBs formed on mica surfaces also promote Aβ aggregation and fibril formation (Fig. 4c). We therefore conclude that on the mica surface a molecular conformation of GM1 that promotes Aβ aggregation was formed in the region outside the triangular region. Because SPBs accelerating Aβ aggregation were not produced on SiO_2 surfaces for any of the compositions examined, we think that in the present experimental systems, this conformation occurred only on the mica surface.

In the MD calculation for case (c), we first used a liquid-ordered phase as the starting model structure, but this did not yield a stable equilibrium structure within our 10-ns calculation time. When we instead used an interdigitated [41,42] and disordered structure as the starting model, an almost stable equilibrium structure emerged in less than 2 ns. The SPB thickness calculated with that model, however,

Please cite this article as: Y. Mao, et al., Surface-induced phase separation of a sphingomyelin/cholesterol/ganglioside GM1-planar bilayer on mica surfaces and microdomain..., Biochim. Biophys. Acta (2010), doi:10.1016/j.bbamem.2010.03.003

was ≈5.2 nm and continued to increase slightly through 10 ns (Fig. 7) even though the observed thickness was only ≈4 nm. Since we observed Aβ aggregation only on mica surfaces, we think that the interaction between the SPB and the mica surface must be taken into account in MD simulations of the molecular conformation of GM1 that promotes Aβ aggregation.

4.3. Surface-induced phase separation and microdomain molecular conformation

We also observed significant Aβ aggregation with all compositions examined on mica surfaces but not with any compositions examined on SiO_2 surfaces. The muscovite mica crystal is easily cleaved at the K+ ion layer, presenting an atomically flat surface comprising Si, Al, and O atoms that form an array of hexagons with a unit cell length of 0.52 nm [43]. Water molecules are adsorbed by hydrogen bonding to the ditrigonal cavities on the mineral surface [44]. Assuming that hydrogen bonding influences the SPB conformation on the mica surface through the interactions between many hydroxyl groups of GM1 head groups and the water molecules trapped in the ditrigonal cavity of the mica surface, we modeled a 50:50 GM1/CHOL interdigitated and disordered structure sitting on the water layer with fixed O atoms positioned at the ditrigonal cavity with 0.52-nm spacing. When we used this as the starting model for an MD calculation (Fig. 7a), in less than 2 ns, the SPB thickness reached a stable value, ≈4.3 nm, close to the observed value, ≈4 nm (Fig. 7b, data II, and Fig. 6c). In these stable structures, the gap between the SPB and the ditrigonal water layer (here we defined it as the distance between the N atom of the GM1 head group in the lower leaflet and the O atom layer of the water layer) was 1–3 nm, which varied temporally and spatially.

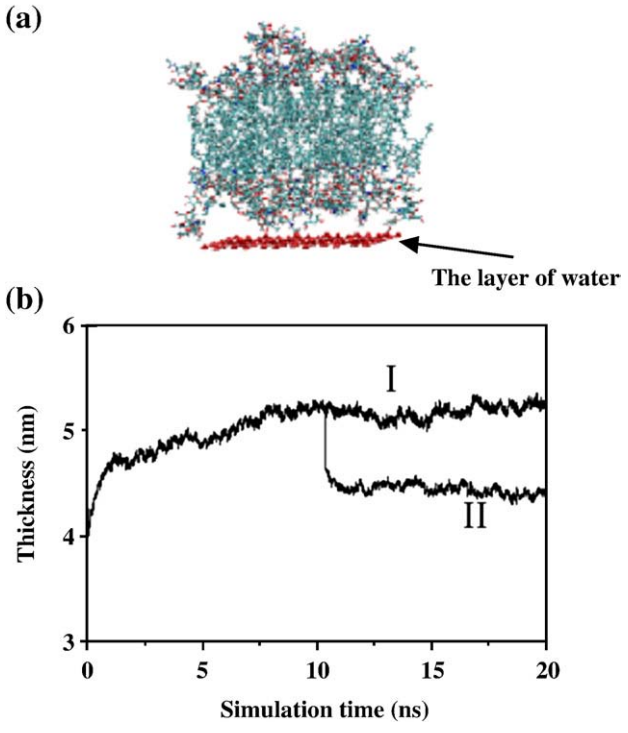

Fig. 7. The MD calculations for the molecular conformation of SPBs outside of the triangular region (area B in Fig. 1b and c). (a) Starting model of the calculation, including the substrate effects. CHOL/GM1 (50:50)-SPB sitting on a layer of water molecules trapped in the ditrigonal cavities with 0.52-nm spacing of the mica surface. Coordinates obtained by 10-ns calculation without substrate effects (data I in b) were used as the starting values of the SPB coordinates. (b) Time lapse of the calculated thickness of the SPB. I: simulation without substrate effects. II: simulation with substrate effects.

To understand the observed phase separation on the mica surface in more detail, we calculated the molecular conformations of SPBs with four extremely low GM1 densities; that is, for 2 GM1 + 30 SM + 32 CHOL, for 4 GM1 + 28 SM + 32 CHOL, for 6 GM1 + 26 SM + 32 CHOL, and for 8 GM1 + 24 SM + 32 CHOL (where the integers are the numbers of molecules in the bilayer) as shown in Fig. 8 and Fig. S5. The results of the simulation show that GM1 molecules aggregate, forming a cluster, and the molecular conformations of GM1 are not interdigitated and disordered, but are close to a "standing" head group structure in these low-concentration regions as shown in Fig. 8a, b, and c. These clusters move in the liquid of the SM/CHOL bilayer, changing their conformations dynamically. The present simulation, however, does not give information about the relation between the cluster size and the GM1 concentration, due to the limited size of the model system used (≈6 nm × 6 nm, containing 64 molecules). However, according to the measured relation reported in ref. [31] observed for GM1-containing POPC bilayers formed on the planar borosilicate glass substrates, the mean size of the GM1 clusters increases with increasing concentration, from 7.3 nm at 0.1 mol% to 19.5 nm at 10 mol% GM1. It is reasonable to assume that the present systems show a similar tendency because both are liquid phases and the main force driving cluster formation is hydrogen bonding and the hydrophobic interactions of GM1 molecules. Therefore, the results of the present computer simulations (shown in Fig. 6c and Fig. 8a, b, and c) show that on the mica surface, the molecular conformations of microdomains containing GM1 have "standing" head groups of GM1 at low GM1 concentrations and that these conformations change into interdigitated and disordered conformations at higher GM1 concentrations. In the present experimental range, from 5% to 50% GM1, the mean cluster size is expected to be much larger than the size of the model system shown in Fig. 6c (≈ 6 nm) [31]. In the present experiments, small GM1 clusters like those reported in ref. [31] were not observed by AFM measurements. This may be because the present three compositions system is more complex compared with the ref. [31] case and the small clusters that have different thickness depending on the size move in the liquid phase.

The mechanism of the surface-induced phase separation on mica surfaces is as follows. At all concentrations examined (5–50 mol% GM1), the mean size of GM1 clusters is much larger than the model system shown in Fig. 6c. Therefore, because the GM1 cluster size has some statistical distribution [31], the present SPBs on the mica surface contain many GM1-rich microdomains having interdigitated and disordered conformations and a small number of small-size GM1 clusters having "standing" head group conformations. Because the larger microdomains are more stable because of the interaction between the GM1 head groups and the water molecules adsorbed in the ditrigonal cavities of the mica surface, the GM1-rich domains coalesce and become larger with increasing GM1 density, resulting in clearer phase separation. The large triangular region observed for the case of 20 mol% GM1 seemed to form through both epitaxial growth effects due to surface-induced phase separation (stabilization) and the triangle symmetry nature of the microstructure of the SM-rich domain (Fig. 6f). The appearance of this large triangular region depended sensitively on the experimental conditions.

The diffusion constant in mica is about twice that in glass [45], but the difference in the phase separation is thought to be due not only to the different diffusion speeds, since no phase separations were not observed on SiO_2 surfaces even after long incubations (>12 h) at 37 °C. We think that the observed difference between the phase separations observed on the SiO_2 and mica surfaces is due both to the large difference in diffusion speed and to interaction with a mica surface water layer having ditrigonal symmetry.

Thus, this analysis provides a good explanation for the observed fact that the "standing" head groups and the interdigitated disordered conformations were observed inside (SM-rich) and outside (GM1-rich) areas of the triangular regions in Fig. 1b or c, respectively.

Please cite this article as: Y. Mao, et al., Surface-induced phase separation of a sphingomyelin/cholesterol/ganglioside GM1-planar bilayer on mica surfaces and microdomain..., Biochim. Biophys. Acta (2010), doi:10.1016/j.bbamem.2010.03.003

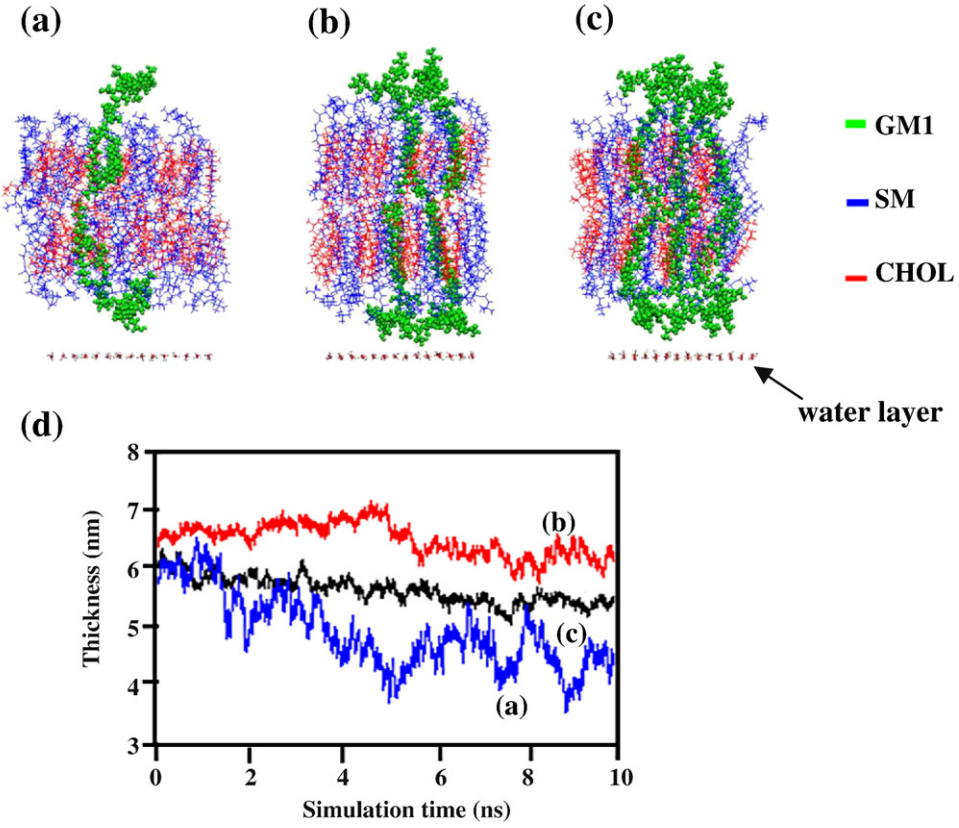

Fig. 8. Equilibrium-state SPBs on a mica surface, obtained by MD computer simulation for the extremely low concentrations of GM1 with consideration for the interaction with water molecules adsorbed in the ditrigonal cavities on the mica surface. (a) 2 GM1 + 30 SM + 32 CHOL, (b) 4 GM1 + 28 SM + 32 CHOL, (c) 6 GM1 + 26 SM + 32 CHOL. Time lapses of the calculated thickness of these SPBs are, respectively, shown in panel (d) by the lines a, b, and c. GM1 molecules move in the liquid phase of SM/CHOL SPBs forming clusters but the thickness of the cluster becomes almost stable after about 5 ns of simulation time.

Because the Aβ aggregation resulting from high-speed unidirectional fibril formation occurred only in the GM1-rich domains (Fig. 4b), we conclude that high-speed Aβ aggregation is induced by the interdigitated and disordered conformations.

We can understand the physical meaning of the lipid bilayer structure shown in Fig. 6g by examining the detailed molecular structure of GM1. The conformation of the GM1 molecule is easily altered by the internal rotation around a chemical bond formed by the carbon sp3 orbitals; that is, around the molecular axes of ceramideC1′-C2′, ceramideC1′-Glcβ1O, Glcβ1O-GlcC1, GlcC4-Galβ1O, and Galβ1O-GalC1, and around similar axes between Galβ, Neu5Acα, GalNAcβ, and Ext. Galβ molecules. Here the GM1 molecule is Ext.Galβ(1-3)GalNAcβ(1-4)[Neu5Acα(2-3)]Galβ(1-4)Glcβ(1-1′)ceramide. If the bilayer does not contain SM, GM1 molecules bend at the boundary between the head group and the ceramide part because of the significant size mismatch between GM1 and CHOL. CHOL molecules then fill the space between GM1 molecules, forming hydrogen bonds with the saccharide residues and the ceramide. The interdigitated and disordered structures in the hydrophobic region are also induced by the large length mismatch between GM1 and CHOL and by the influence of the interaction between the GM1 head group and the water layer adsorbed in the ditrigonal cavities of the mica surface. We therefore think that the interdigitated and disordered structure is a conformation of GM1/CHOL bilayers that appears because of the clustering effects of GM1 molecules and the strong interaction between GM1 head groups and a water layer trapped by the ditrigonal cavities on the mica surface. The results of the MD simulation are consistent with our observations in that they indicate that the lipid bilayer is in the liquid phase.

In future work, we plan to carry out MD simulations investigating the interaction between GM1 and Aβ molecules in detail in order to find out why the GM1 conformation identified in the present study promotes Aβ aggregation. Among the results presented here, however, are some suggestions as to why this conformation would promote aggregation. We know from the calculated results that the area of the reactive sugar moiety exposed to the SPB surface is much larger in the case of the mica surface and that it changes with time. Amyloid beta is thought to interact with sialic-acid-rich (multivalent) regions of cell surfaces [12]. In the molecular conformation of GM1 shown in Fig. 6g, the reactive sialic acid moiety (neuraminic acid) of the GM1 head group is significantly exposed to the SPB surface and induces the extremely high speed of aggregations.

5. Conclusions

Using AFM, FM, and MD simulations, we investigated the interaction between Aβ and GM1/SM/CHOL SPBs formed on mica and SiO_2 surfaces and found that the interaction differs depending on the surface. On the mica surface, a surface-induced phase separation forms GM1 clusters that have an interdigitated and disordered molecular conformation at all GM1 concentrations examined, and especially SM-rich triangular regions surrounded by GM1-rich domains are clearly formed when the SPBs contain 20 mol% GM1. The present analysis shows that the rapid Aβ aggregation, which resulted in the formation of many fibril agglomerates, is induced by this molecular conformation of GM1 on the mica surface, where phase separation is induced mainly by the clustering nature of GM1 molecules and the strong interactions between GM1 head groups and water molecules adsorbed in the ditrigonal cavities on the mica surface. On the SiO_2 surface, on the other hand, a homogeneous planar bilayer was formed and globular Aβ agglomerates were generated, but the aggregation was much slower than that on the mica surface.

Please cite this article as: Y. Mao, et al., Surface-induced phase separation of a sphingomyelin/cholesterol/ganglioside GM1-planar bilayer on mica surfaces and microdomain..., Biochim. Biophys. Acta (2010), doi:10.1016/j.bbamem.2010.03.003

The formation of triangular regions, which is only the result of coalescence, is not essential to the rapid formation of Aβ fibrils, and 20% GM1 is not a physiological concentration (too high). We, however, acknowledge that 40:40:20 mol% has become an interesting guide to find an interesting conformation of SPB containing GM1. But this is only the first step towards making in vivo predictions. We think that the detailed knowledge of the GM1 molecular conformation that significantly accelerates Aβ aggregation will be useful to researchers investigating Aβ–GM1 interactions.

Acknowledgments

We appreciate the helpful comments of Prof. Matsuzaki at Kyoto University. This work was partly supported by Grants-in-Aid for Scientific Research, Basic research (A) promoted by the Japanese Ministry of Education, Culture, Sports, Science, and Technology, by the JSPS Asian Core Program, by the NINS Cooperation Project "Biomolecular Sensors", by IMS special research projects, and by JST, CREST.

Appendix A. Supplementary data

Supplementary data associated with this article can be found, in the online version, at doi:10.1016/j.bbamem.2010.03.003.

References

[1] C.L. Schengrund, The role(s) of gangliosides in neural differentiation and repair: a perspective, Brain Res. Bull. 24 (1990) 131–141.
[2] S. Ngamukote, M. Yanagisawa, T. Ariga, S. Ando, R.K. Yu, Developmental changes of glycosphingolipids and expression of glycogenes in mouse brains, J. Neurochem. 103 (2007) 2327–2341.
[3] K. Yanagisawa, A. Odaka, N. Suzuki, Y. Ihara, GM1 ganglioside-bound amyloid β-protein (Aβ): a possible form of preamyloid in Alzheimer's disease, Nat. Med. 1 (1995) 1062–1066.
[4] L.P. Choo-Smith, W. Garzon-Rodriguez, C.G. Glabe, W.K. Surewicz, Acceleration of amyloid fibril formation by specific binding of Aβ-(1–40) peptide to ganglioside-containing membrane vesicles, J. Biol. Chem. 272 (1997) 22987–22990.
[5] A. Kakio, S. Nishimoto, K. Yanagisawa, Y. Kozutsumi, K. Matsuzaki, Cholesterol-dependent formation of GM1 ganglioside-bound amyloid β-protein, an endogenous seed for Alzheimer amyloid, J. Biol. Chem. 276 (2001) 24985–24990.
[6] A. Kakio, S. Nishimoto, K. Yanagisawa, Y. Kozutsumi, K. Matsuzaki, Interactions of amyloid β-protein with various gangliosides in raft-like membranes: importance of GM1 ganglioside-bound form as an endogenous seed for Alzheimer amyloid, Biochemistry 41 (2002) 7385–7390.
[7] M. Wakabayashi, T. Okada, Y. Kozutsumi, K. Matsuzaki, GM1 ganglioside-mediated accumulation of amyloid beta-protein on cell membranes, Biochem. Biophys. Res. Commun. 328 (2005) 1019–1023.
[8] N. Yamamoto, Y. Fukata, M. Fukata, K. Yanagisawa, GM1-ganglioside-induced Aβ assembly on synaptic membranes of cultured neurons, Biochim. Biophys. Acta 1768 (2007) 1128–1137.
[9] T. Okada, M. Wakabayashi, K. Ikeda, K. Matsuzaki, Formation of toxic fibrils of Alzheimer's amyloid β-protein-(1–40) by monosialoganglioside GM1, a neuronal membrane component, J. Mol. Biol. 371 (2007) 481–489.
[10] N. Yamamoto, E. Matsubara, S. Maeda, H. Minagawa, A. Takashima, W. Maruyama, M. Michikawa, K. Yanagisawa, A ganglioside-induced toxic soluble Aβ assembly: its enhanced formation from Aβ bearing the arctic mutation, J. Biol. Chem. 282 (2007) 2646–2655.
[11] E.Y. Chi, S.L. Frey, K.Y.C. Lee, Ganglioside GM1-mediated amyloid-beta fibrillogenesis and membrane disruption, Biochemistry 46 (2007) 1913–1924.
[12] C.B. Cowan, G.L. Coté, T.A. Good, Development of photocrosslinked sialic acid containing polymers for use in Aβ toxicity attenuation, Biomaterials 29 (2008) 3408–3414.
[13] J. McLaurin, T. Franklin, P.E. Fraser, A. Chakrabartty, Structural transitions associated with the interaction of Alzheimer β-amyloid peptides with gangliosides, J. Biol. Chem. 273 (1998) 4506–4515.
[14] P.Y. Chen, C.C. Lin, Y.T. Chang, S.C. Lin, S.I. Chan, One O-linked sugar can affect the coil-to-β structural transition of the prion peptide, Proc. Natl. Acad. Sci. U. S. A. 99 (2002) 12633–12638.
[15] P.H. Nguyen, M.S. Li, G. Stock, J.E. Straub, D. Thirumalai, Monomer adds to preformed structured oligomers of Aβ-peptides by a two-stage dock–lock mechanism, Proc. Natl. Acad. Sci. U. S. A. 104 (2007) 111–116.
[16] L. Cruz, B. Urbanc, J.M. Borreguero, N.D. Lazo, D.B. Teplow, H.E. Stanley, Solvent and mutation effects on the nucleation of amyloid β-protein folding, Proc. Natl. Acad. Sci. U. S. A. 102 (2005) 18258–18263.
[17] W. Han, Y.D. Wu, Molecular dynamics studies of hexamers of amyloid-β peptide (16–35) and its mutants: influence of charge states on amyloid formation, Proteins 66 (2007) 575–587.
[18] A. Olofsson, M. Lindhagen-Persson, A.E. Sauer-Eriksson, A. Öhman, Amide solvent protection analysis demonstrate that Amyloid(beta)(1–40) and Amyloid(beta)(1–42) form different fibrillar structures under identical conditions, Biochem. J. 404 (2007) 63–70.
[19] A.T. Petkova, W.M. Yau, R. Tycko, Experimental constraints on quaternary structure in Alzheimer's beta-amyloid fibrils, Biochemistry 45 (2006) 498–512.
[20] M. Arimon, I. Díez-Pérez, M.J. Kogan, N. Durany, E. Giralt, F. Sanz, X. Fernàndez-Busquets, Fine structure study of Aß1–42 fibrillogenesis with atomic force microscopy, FASEB J. 19 (2005) 1344–1346.
[21] I. Mastrangelo, M. Ahmed, T. Sato, W. Liu, C. Wang, P. Hough, S.O. Smith, High resolution atomic force microscopy of soluble Ab42 oligomers, J. Mol. Biol. 358 (2006) 106–119.
[22] K. Simons, E. Ikonen, Functional rafts in cell membranes, Nature 387 (1997) 569–572.
[23] K. Bacia, D. Scherfeld, N. Kahya, P. Schwille, Fluorescence correlation spectroscopy relates rafts in model and native membranes, Biophys. J. 87 (2004) 1034–1043.
[24] B. Chini, M. Parenti, G-protein coupled receptors in lipid rafts and caveolae: how, when and why do they go there? J. Mol. Endocrinol. 32 (2004) 325–338.
[25] W.H. Binder, V. Barragan, F.M. Menger, Domains and rafts in lipid membranes, Angew. Chem. Int. Ed. 42 (2003) 5802–5827.
[26] R.G. Parton, Ultrastructural localization of gangliosides; GM1 is concentrated in caveolae, J. Histochem. Cytochem. 42 (1994) 155–166.
[27] E. Sackmann, Supported membranes: scientific and practical applications, Science 271 (1996) 43–48.
[28] J.J. Shi, T.L. Yang, P.S. Cremer, Multiplexing ligand-receptor binding measurements by chemically patterning microfluidic channels, Anal. Chem. 80 (2008) 6078–6084.
[29] W.J. Galush, J.A. Nye, J.T. Groves, Quantitative fluorescence microscopy using supported lipid bilayer standards, Biophys. J. 95 (2008) 2512–2519.
[30] M.B. Forstner, C.K. Yee, A.N. Parikh, J.T. Groves, Lipid lateral mobility and membrane phase structure modulation by protein binding, J. Am. Chem. Soc. 128 (2006) 15221–15227.
[31] J. Shi, T. Yang, S. Kataoka, Y. Zhang, A.J. Diaz, P.S. Cremer, GM1 clustering inhibits cholera toxin binding in supported phospholipid membranes, J. Am. Chem. Soc. 129 (2007) 5954–5961.
[32] M.L. Kraft, P.K. Weber, M.L. Longo, I.D. Hutcheon, S.G. Boxer, Phase separation of lipid membranes analyzed with high-resolution secondary ion mass spectrometry, Science 313 (2006) 1948–1951.
[33] Y.F. Dufrêne, G.U. Lee, Advances in the characterization of supported lipid films with the atomic force microscope, Biochim. Biophys. Acta 1509 (2000) 14–41.
[34] S.A. Contera, V. Lemaitre, M.R.R. de Planque, A. Watts, J.F. Ryan, Relating structure, biomechanics and function of single membrane proteins, Biophys. J. 89 (2005) 3129–3140.
[35] W. Humphrey, A. Dalke, K. Schulten, VMD: visual molecular dynamics, J. Mol. Graph. 14 (1996) 33–38.
[36] Y.L. Mao, R. Tero, Y. Imai, T. Hoshino, T. Urisu, The morphology of $GM1_x/SM_{0.6-x}/Chol_{0.4}$ planar bilayers supported on SiO_2 surfaces, Chem. Phys. Lett. 460 (2008) 289–294.
[37] Wu. E-S, K. Jacobson, D. Papahadjopoulos, Lateral diffusion in phospholipid multibilayers measured by fluorescence recovery after photobleaching, Biochemistry 16 (1977) 3936–3941.
[38] A. Ferraretto, M. Pitto, P. Palestini, M. Masserini, Lipid domains in the membrane: thermotropic properties of sphingomyelin vesicles containing GM1 ganglioside and cholesterol, Biochemistry 36 (1997) 9232–9236.
[39] C. Yuan, L.J. Johnston, Atomic force microscopy studies of ganglioside GM1 domains in phosphatidylcholine and phosphatidylcholine/cholesterol bilayers, Biophys. J. 81 (2001) 1059–1069.
[40] G.M. Shankar, S. LI, T.H. Mehta, A. Garcia-Munoz, N.E. Shepardson, I. Smith, F.M. Brett, M.A. Farrell, M.J. Rowan, C.A. Lemere, C.M. Regan, D.M. Walsh, B.L. Sabatini, D.J. Selkoe, Amyloid-β protein dimers isolated directly from Alzheimer's brains impair synaptic plasticity and memory, Nat. Med. 14 (2008) 837–842.
[41] M. Yamazaki, M. Miyazu, T. Asano, A. Yuba, N. Kume, Direct evidence of induction of interdigitated gel structure in large unilamellar vesicles of dipalmitoylphosphatidylcholine by ethanol: studies by excimer method and high-resolution electron cryomicroscopy, Biophys. J. 66 (1994) 729–733.
[42] C. Huang, T.J. McIntosh, Probing the ethanol-induced chain interdigitations in gel-state bilayers of mixed-chain phosphatidylcholines, Biophys. J. 72 (1997) 2702–2709.
[43] T. Fukuma, K. Kobayashi, K. Matsushige, H. Yamada, True atomic resolution in liquid by frequency-modulation atomic force microscopy, Appl. Phys. Lett. 87 (2005) 034101–034103.
[44] S.H. Park, G. Sposito, Structure of water adsorbed on a mica surface, Phys. Rev. Lett. 89 (2002) 085501–085503.
[45] E.I. Goksu, B.A. Nellis, W.-C. Lin, J.H. Satcher Jr., J.T. Groves, S.H. Risbud, M.L. Longo, Effect of support corrugation on silica xerogel-supported phase-separated lipid bilayers, Langmuir 25 (2009) 3713–3717.

Please cite this article as: Y. Mao, et al., Surface-induced phase separation of a sphingomyelin/cholesterol/ganglioside GM1-planar bilayer on mica surfaces and microdomain..., Biochim. Biophys. Acta (2010), doi:10.1016/j.bbamem.2010.03.003